Dalton Transactions

Accepted Manuscript

ROYAL SOCIETY OF CHEMISTRY

www.rsc.org/dalton

A Sterically Stabilized Fe^{I}-Fe^{I} Semi-Rotated Conformation of [FeFe] Hydrogenase Subsite Model

Roman Goy,[a] Luca Bertini,*[c] Catherine Elleouet,[d] Helmar Görls,[a] Giuseppe Zampella,[c] Jean Talarmin,[d] Luca De Gioia,*[c] Philippe Schollhammer,*[d] Ulf-Peter Apfel,*[b] Wolfgang Weigand*[a,e]

Abstract

The [FeFe] hydrogenase is a highly sophisticated enzyme for the synthesis of hydrogen via a biological route. The *rotated state* of the H-cluster in the [$Fe^{I}Fe^{I}$] form was found to be an indispensible criteria for an effective catalysis. Mimicking the specific rotated geometry of the [FeFe] hydrogenase active site is highly challenging as no protein stabilization is present in model compounds. In order to simulate the sterical demanding environment of the nature's active site, the sterically crowded *meso*-bis(benzylthio)diphenylsilane (**2**) was utilized as dithiolate linker in an [2Fe2S] model complex. The reaction of the obtained hexacarbonyl complex **3** with 1,2-bis(dimethylphosphino)ethane (dmpe) results three different products depending on the amount of dmpe used in this reaction: [{$Fe_2(CO)_5${μ-$(SCHPh)_2SiPh_2$}}$_2$(μ-dmpe)] (**4**), [$Fe_2(CO)_5$(κ^2-dmpe){μ-$(SCHPh)_2SiPh_2$}] (**5**) and [$Fe_2(CO)_5$(μ-dmpe){μ-$(SCHPh)_2SiPh_2$}] (**6**). Interestingly, the molecular structure of compound **5** shows a [FeFe] subsite comprising a semi-rotated conformation, which was fully characterized as well as the other isomers **4** and **6** by elemental analysis, IR and NMR spectroscopy, X-ray diffraction analysis (XRD) and DFT calculations. The herein reported model complex is the first example so far reported for [$Fe^{I}Fe^{I}$] hydrogenase model complex showing a semi-rotated geometry without the need of stabilization via agostic interactions (Fe···H-C).

Introduction

[FeFe] hydrogenases are the most efficient proton reducing catalysts and enable the generation of dihydrogen in nature.[1–3] Numerous structural as well as functional studies on [2Fe2S] as well as their homologous [2Fe2E] (E = Se, Te) complexes as [FeFe]-H_2ase mimics were performed for a better understanding of its active site.[4–18] As independently reported by Peters as well as Fontecilla-Camps *et al*., the active site of this enzyme contains a $[2Fe]_H$ subsite covalently linked by a cysteine bridge to a [4Fe4S] ferredoxin cluster (Figure 1).[19–21] The diiron center is best described as rotated state that possesses a square pyramid geometry at one iron atom (Fe_d, Figure 1) and is inverted with respect to the geometry of the other moiety (Fe_p, Figure 1).[22] This causes a free coordination site at the apical site of the distal iron moiety (Fe_d), where protons and molecular hydrogen are proposed to bind during the catalytic process of production and uptake of H_2. Mimicking of this specific geometry in synthetic [FeFe]-H_2ase models is highly challenging and only specific states of the H_2-formation mechanism are accessible.[23–26] Mechanistic details of the natural process were intensively investigated by Lubitz *et al.* with EPR spectroscopy and helped synthetic chemists in targeting specific intermediates.[22,27–29] Especially, the rotated state was found to be an indispensible criteria for active compounds[22] and for the formation of stabilized terminal hydrides. Notably, although Happe, Lubitz and Fontecave *et al*. showed the successful incorporation of artificial aminodithiolato derived model complexes into the protein environment with full activity towards H_2 generation, these complexes do show a different chemistry under electrocatalytic conditions.[30,31] Although spectroscopic data pointing towards formation of rotated states in oxidized and reduced model compounds was reported,[10,32] Darensbourg *et al*. were the first to provide structural evidence for a mixed-valent [$Fe^{I}Fe^{II}$] complex with a rotated geometry.[14] Model complexes comprising a [$Fe^{I}Fe^{I}$] moiety with such a rotated geometry are rare. Only very recently, the first examples of [$Fe^{I}Fe^{I}$]-H_2ase mimics featuring a fully rotated conformation, [$Fe_2(CO)_4$(κ^2-dmpe){μ-$(SCH_2)_2$N-Bn}][23] (Bn = Benzyl) and [$Fe_2(CO)_4$(κ^2-dppv){μ-$(SCH_2)_2CEt_2$}][24] were

reported simultaneously. Remarkably, both complexes reveal similar structural features that were reported to be crucial for the stabilization of this particular structure, i.e. an asymmetrical disubstituted diiron center, a bulky dithiolate bridge and an intramolecular remote agostic interaction.

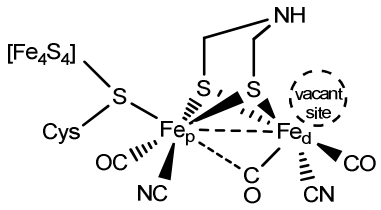

Fig. 1: Active site of [FeFe]-Hydrogenase with the vacant site located at the distal iron (Fe_d).

Inspired by these new findings and in continuation of our research on silicon containing [FeFe] hydrogenase model complexes, we investigated the reactivity of 1,2-bis(dimethylphosphino)ethane (dmpe) with diiron derivatives featuring sterically demanding silicon bridges.[32–35] Silicon species thereby have numerous advantages as the starting materials, R_2SiCl_2 are commercially available in great variety and can be easily modified at the central silicon position. Herein, we report the synthesis and the molecular structure of a [Fe^IFe^I] model complex having a strongly distorted conformation. In contrast to [$Fe_2(CO)_4(\kappa^2$-dmpe){μ-$(SCH_2)_2$N-Bn}][23] and [$Fe_2(CO)_4(\kappa^2$-dppv){μ-$(SCH_2)_2CEt_2$}][24], no intramolecular remote agostic interaction is observed and required. The identification of this species with its structural features along with DFT computations corroborates the theory[23,24,36] that in contrast to earlier reports the simultaneous presence of the three proposed structural factors (asymmetrical coordination at the two Fe atoms, bulky size of the dithiolate bridgehead, weak remote agostic interaction Fe···H-C) to obtain partially or semi-rotated structures of diiron(I) dithiolates[14] is not mandatory. However, each of the three factors is crucial for observing a full-rotated geometry at a single Fe atom, as that present in the [FeFe] hydrogenase cofactor.

Results and Discussion

In order to enforce an inverted geometry and to avoid "flipping" of the S-to-S linker in [2Fe2S]-clusters, the sterically crowded dithiol *meso*-bis(benzylthio)diphenylsilane was synthesized according to scheme 1 in a modified procedure described by Zubieta *et al.*.[37] Dichlorodiphenylsilane was reacted with benzylmercaptan in the presence of *n*-butyllithium, whereas compound **1** was generated. *In situ* treatment of **1** with *tert.*-butyllithium induces a double Wittig-rearrangement affording **2** as a mixture of the *d-* , *l-* and *meso*-forms. Crystallization from hexane exclusively yields the *meso*-form as the major product in 61 % yield. Since compound **2** is not described in literature, its absolute configuration was established by single crystal X-ray analyses, as depicted in Figure S1. Reaction of [$Fe_3(CO)_{12}$] and *meso*-bis(benzylthio)diphenylsilane **2** in refluxing toluene afforded the corresponding [$Fe_2(CO)_6${μ-$(SCHPh)_2SiPh_2$}] (**3**) within one hour in 64% yield (Scheme 1). Complex **3** was characterized by ^{1}H, ^{13}C{^{1}H}, HSQC, ^{1}H,^{1}H-COSY NMR spectroscopy, as well as by elemental analysis and mass spectrometry. Crystals suitable for single crystal X-ray analysis were obtained by cooling an acetonitrile solution of **3** to -20°C. Complex **3** exhibits a typical [2Fe2S] core with a "butterfly arrangement", whereas the geometry around each iron atoms can be best described as a distorted square pyramidal supplemented by a Fe-Fe single bond (Figure S2). As reported for analogous complexes with a silane- as well as tin-functionalized dithiolate bridge the bond angles S-C-Si deviate strongly from the ideal angle of 109.45° (see values in Figure S2).[32–35,38]

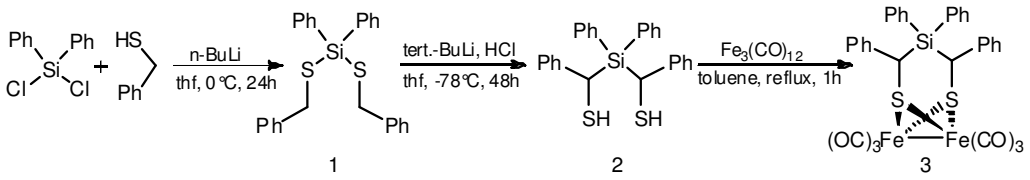

Scheme 1: Synthesis of *meso*-bis(benzylthio)diphenylsilane *via* double Wittig-rearrangement and complexation to afford **3**.

Since it has recently been shown that the introduction of a bulky S-to-S linker together with a asymmetrical substitution with a bidentate phosphine could favor a "rotated state",[23,24] complex **3** was reacted with 1,2-bis(dimethylphosphino)ethane (dmpe) (Scheme 2). This reaction was performed in refluxing THF for 20 minutes and afforded three different products, [{$Fe_2(CO)_5${μ-$(SCHPh)_2SiPh_2$}}$_2$(μ-dmpe)] (**4**), [$Fe_2(CO)_5$(κ^2-dmpe){μ-$(SCHPh)_2SiPh_2$}] (**5**), [$Fe_2(CO)_5$(μ-dmpe){μ-$(SCHPh)_2SiPh_2$}] (**6**). The yields of each compound strongly depend on the reaction conditions (see scheme 2 and experimental part). If one equivalent dmpe based on complex **3** is used in this reaction, compound **4** is observed as the main product in 17 % yield, whereas **6** can be obtained in 3 % yield and the chelated isomer **5** just in traces, viewed as light purple band at the silica column chromatography of the crude product. Switching to two equivalents of dmpe based on complex **3** changes the yields dramatically. Isomer **6** is now observed as the main product with 35 % and complex **5** with 7 % yield. Compound **4** can just be obtained in traces, to be observed as a light red band at the column. Elongation of the reaction time decreases the yield of complex **5** to nearly 0 %. All compounds were characterized by elemental analysis, IR, NMR spectroscopy and X-ray diffraction analysis (XRD). Red crystals of **4** and **6** suitable for XRD analysis were obtained by evaporation of a hexane solution at 20 °C (Figures 2 and 3 right, respectively). Purple crystals of **5** were obtained by slow diffusion of *n*-pentane into a solution of **5** in toluene at 8 °C (Figure 3 left).

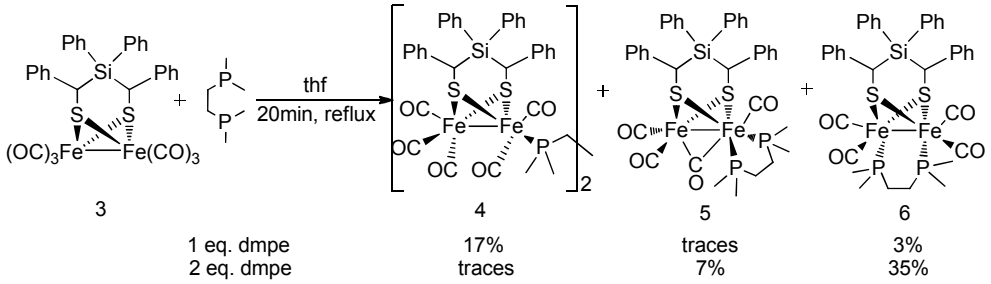

Scheme 2: Synthesis of dmpe-substituted complexes **4**, **5** and **6** in refluxing THF.

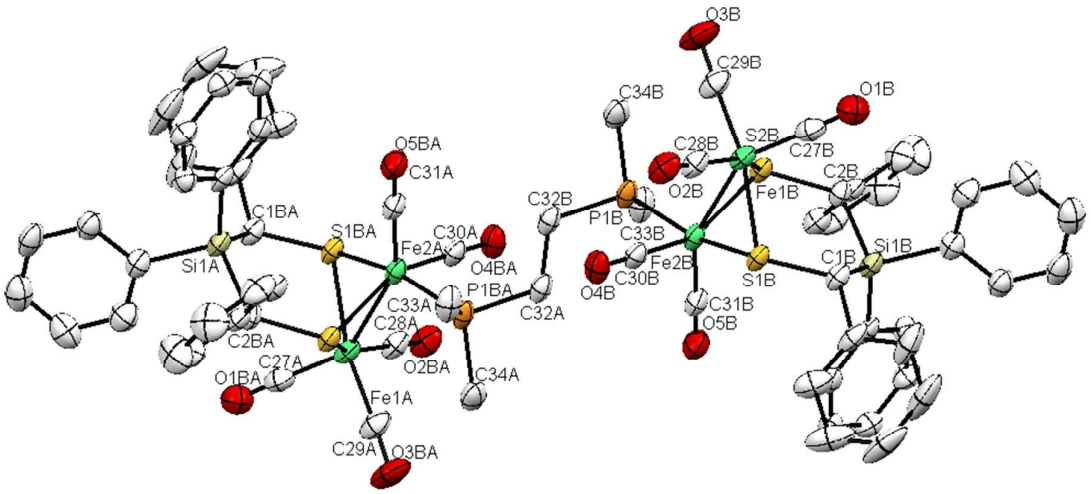

Fig. 2: Molecular structure of compound **4**, which is reduced to one of two independent dimer molecules in the unit cell with an inversion center localized at the C32A-C32B-bond. Hydrogens are omitted for clarity. Selected bond lengths [Å] and angles [°]: Fe1B-Fe2B 2.5526(12), Fe2B-P1B 2.2377(15), P1B-C32B 1.837(6), C32B-C32A 1.531(12), Fe1B-Fe2B-P1B 109.61(6), P1B-C32B-C32A 114.6(5).

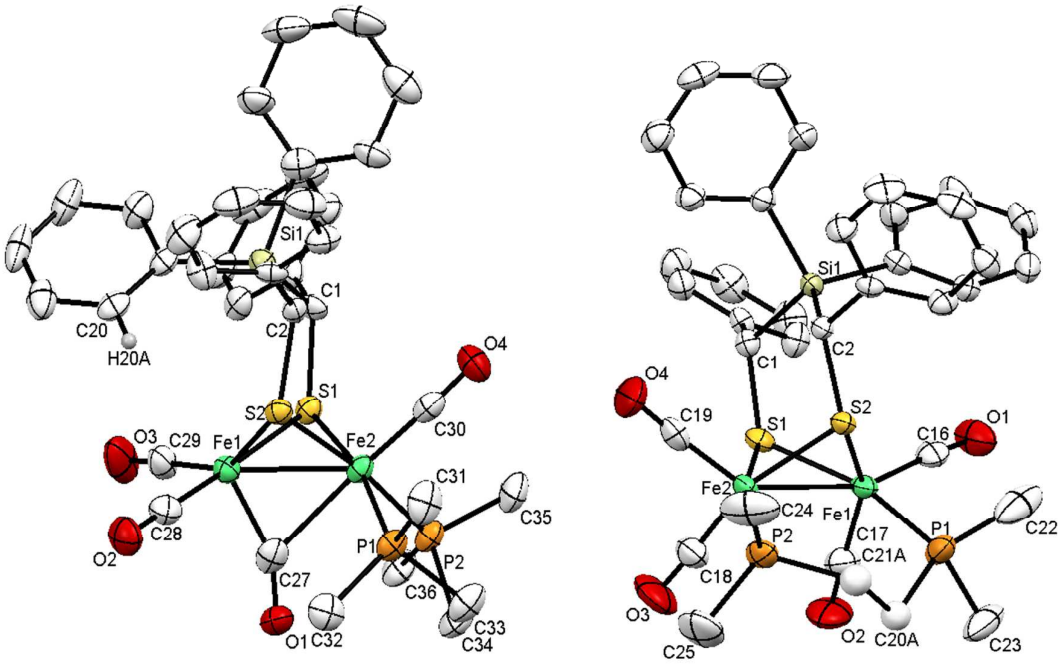

Fig. 3: Molecular structures of chelated isomer **5** (left) and bridged isomer **6** (right). Selected bond lengths [Å] and angles [°]: **5**: Fe1-Fe2 2.5450(15), Fe1-C27 1.789(9), Fe2-C27 2.379(9), Fe1-H20A 3.176. **6**: Fe1-Fe2 2.5238(7), Fe1-P1 2.2101(11), Fe2-P2 2.2174(11), Fe1-P1-C20A 118.9(2), Fe2-P2-C21A 117.7(3).

Two crystallographically independent molecules of compound **4** are found in the triclinic unit cell. The molecular structure of **4** reveals that this species features two $\{Fe_2(CO)_5\{\mu\text{-}(SCHPh)_2SiPh_2\}_2$ moieties bridged by a dmpe ligand with an inversion center localized at the C32A-C32B-bond. Molecular structures of analogous compounds have been already reported.[36,39,40] It is, however, worth noting that in the case of **4** the phosphorus atoms of the diphosphine are bound in basal position while in

other reported molecular structures an apical binding mode is observed.[9,39,40] Complexes **5** and **6** are two structural isomers that differ by the coordination mode of the bidentate ligand dmpe. The structure of **6** is very similar to those reported for analogous complexes.[36,40,41] As it is shown in Figure 3, the structure reveals an eclipsed structure in the solid state unlike compound **5** and the dmpe is bridged in a dibasal position. The sterically bulky *meso*-bis(benzylthio)diphenylsilane induce a slight distortion around the two iron atoms evidenced by a significant difference between the two angles C19-Fe2-Fe1 (145.52°) and C16-Fe1-Fe2 (157.15). The IR spectrum of **6** (Fig. 4) shows a typical set of four carbonyl bands at 1987 (s), 1950 (vs), 1917 (s) and 1899 cm^{-1} (m), which are similar to those in other reported complexes with such symmetry.[42–47] The $^{31}P\{^{1}H\}$ NMR spectrum reveals two singlets at 38.70 ppm and 32.58 ppm for the bridging dmpe ligand caused by the asymmetry of the complex. The ^{1}H NMR spectrum displays the expected signal group for a symmetrically bridged dmpe ligand.

Compound **5** features a semi-rotated coordination environment with a strongly distorted square pyramidal edge-shared $\{FeS_2(CO)_3\}$ group with respect to the $\{FeS_2(CO)P_2\}$ moiety. This coordination mode is locked and stabilized by a CO ligand in semi-bridging position. A close inspection of the molecular structure of **5** reveals that its conformation cannot be considered as fully rotated and should be better described as a trigonal bipyramid centered at Fe. An Addison τ parameter (the difference between S2-Fe1-C29 and S1-Fe1-C28 divided by 60) of 0.49 indicates that the structure of **5** is best described as an intermediate of a square-pyramidal and a trigonal bipyramidal geometry around.[48] In contrast to the diiron complexes $[Fe_2(CO)_4(\kappa^2\text{-dmpe})\{\mu\text{-}(SCH_2)_2NBn\}]$ and $[Fe_2(CO)_4(\kappa^2\text{-dppv})\{\mu\text{-}(SCH_2)_2CEt_2\}]$, in which an Fe-H agostic interaction (2.750 Å)[23] was evidenced as a major structural feature for stabilizing a rotated structure,[24] compound **5** lacks such an agostic interaction. In complex **5** is observed a Fe···H interatomic distance of 3.184 Å between the semi-rotated iron atom Fe1 and the closest hydrogen atom H20A, that belongs to a phenyl ring bound to silicon (Figure 3). However, this interatomic distance is too long to be considered as a Fe···H agostic interaction and even as an Fe···H electrostatic interaction.[49] The IR spectra of compound **5** are shown in Figure 4. In the IR spectrum recorded in the solid state a band at 1801 cm^{-1} indicates a bridging CO ligand constrained by crystal packing, while an unrotated conformation of **5** prevails in CH_2Cl_2 solution due to conformational freedom (CH_2Cl_2 was chosen due to the moderate solubility in more or less polar solvents), as only a weak bridging CO ligand stretch can be recognized at 1801 cm^{-1}. A typical set of carbonyl bands at 2007 (s), 1937 (s), 1903 (s) and 1801 cm^{-1} (m) is observed in solution, which are similar to those already reported for $[Fe_2(CO)_4(\kappa^2\text{-dmpe})\{\mu\text{-}(SCH_2)_2NBn\}]$.[23] The $^{31}P\{^{1}H\}$ NMR spectrum reveal just one singlet at 63.13 ppm for the dmpe ligand, which indicates a dibasal coordination. The ^{1}H NMR spectrum displays the expected signal group for such a dmpe ligand substitution; a ^{13}C NMR spectrum could not be recorded due to poorly resolution.

In order to rationalize experimental results, DFT calculations were performed and focused on the relative stability of $\mathbf{5}_{unrot}$, $\mathbf{5}_{semirot}$ and **6** (hereafter the subscript rot, semirot and unrot indicate the rotated, semirotated and non rotated isomers, respectively). The geometry optimizations at BP86/TZVP gas-phase level were carried out using molecular structures as starting point and converged $\mathbf{5}_{semirot}$ to the fully rotated form $\mathbf{5}_{rot}$. $\mathbf{5}_{rot}$ is 1.1 kcal/mol higher in energy as compared to **6**, which is also reflected in the yields of the reaction with dmpe (7 % for **5** and 35 % for **6**) affording the $\mathbf{5}_{unrot}$ isomer as a transition state 3.4 kcal/mol higher in energy. Upon optimization, the structure of **6** does not change significantly (Fe-Fe distance from 2.523 Å (XRD) to 2.563 Å (DFT); C-Fe-Fe-C dihedral angle from 23.8° (XRD) to 10.4° degree (DFT)). The optimized structure of $\mathbf{5}_{rot}$ is much more interesting (Figure 5) as it features a fully rotated state (dihedral angle from 87.1° to 106.3° degree; shorter Fe-μC distance from 2.385 Å to 2.201 Å) with a more symmetrical shape. The Fe···H interatomic distance of the hypothetical agostic interaction decreases to 2.903 Å (-0.281 Å compared to the molecular structure). These two structural features might suggest either that the interaction among the molecules in the crystal prevents the complete rotation of the $Fe(CO)_3$ group in $\mathbf{5}_{semirot}$ or, in the light of experimental observations in solution (loss of rotated form) even the opposite effect, namely that removal of packing forces causes the rearrangement from $\mathbf{5}_{semirot}$ to $\mathbf{5}_{unrot}$. Moreover, the rotation allows a small rearrangement of the Si bidentate ligand and therefore the approaching of the iron and hydrogen atoms.

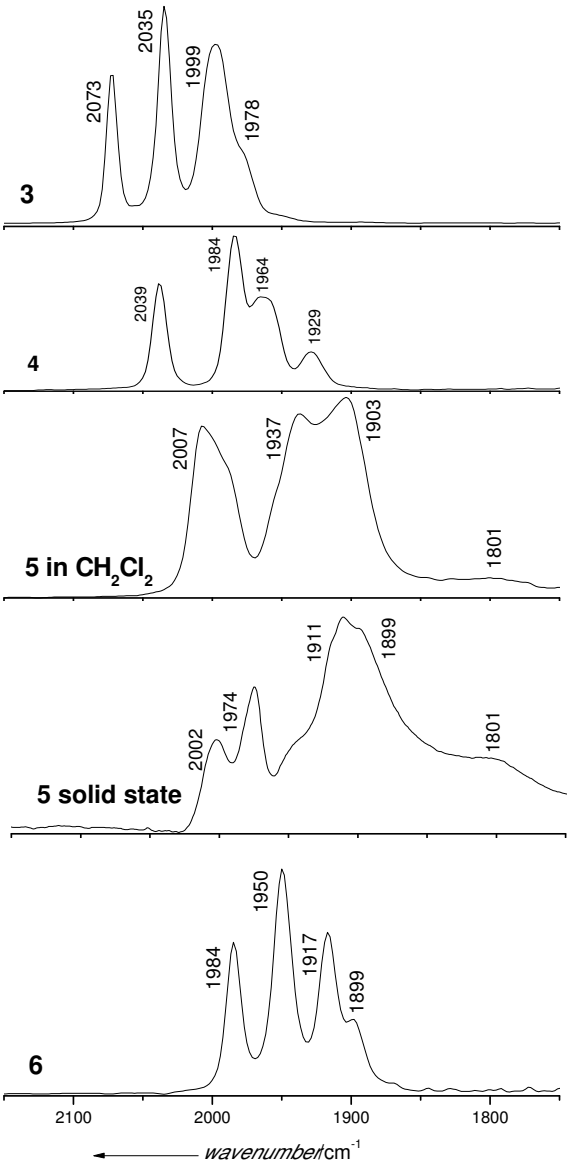

Fig. 4: FTIR spectra of the carbonyl stretching region for compounds **3**, **4**, **5** in CH_2Cl_2 and solid state and **6**.

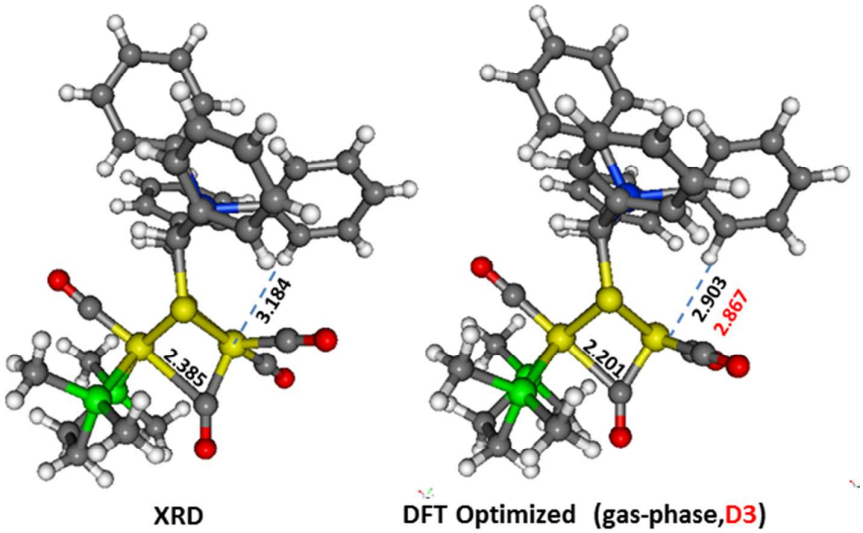

Fig. 5: Comparison of XRD molecular structure and DFT geometry optimized structures at BP86/TZVP gas-phase and D3 dispersion corrected (in red) level for complex **5**. Distances in Å.

Starting from $\mathbf{5}_{\mathbf{unrot}}$ in CH_2Cl_2 solution the optimization converged to $\mathbf{5}_{\mathbf{rot}}$, as well as in the case of B3LYP and BP86/D3 dispersion corrected levels of theory. At BP86/D3 level, the $\mathbf{5}_{\mathbf{unrot}}$ form is not a stationary point on the PES (potential energy surface) and the geometry optimization converges to $\mathbf{5}_{\mathbf{rot}}$. In Table 1 are reported the $\mathbf{5}_{\mathbf{unrot}}/\mathbf{5}_{\mathbf{rot}}$ energy differences.

Table 1. Total energy differences (in kcal/mol) between $\mathbf{5}_{\mathbf{unrot}}$ and $\mathbf{5}_{\mathbf{rot}}$ isomers as a function of the computational level.

	BP86/gas-phase	BP86/CH_2Cl_2	BP86/D3	B3LYP/gas-phase
$\mathbf{5}_{\mathbf{unrot}}$	+3.4	+5.2	$\rightarrow\mathbf{5}_{\mathbf{rot}}$	+3.9
$\mathbf{5}_{\mathbf{rot}}$	0.0	0.0	0.0	0.0

A closer inspection of the geometry optimization energy profile starting from the $\mathbf{5}_{\mathbf{unrot}}$ structure puts in evidence of a semirotated transition state structure similar to $\mathbf{5}_{\mathbf{semirot}}$ whose energy lies in the middle between $\mathbf{5}_{\mathbf{unrot}}$ and $\mathbf{5}_{\mathbf{rot}}$ (Figure 6). In the calculated $\mathbf{5}_{\mathbf{semirot}}$ structure the C-Fe-Fe-C dihedral angle is 72.2°. Depending on the nature of the ligands, in the all-terminal CO form of hydrogenase model complexes this dihedral angle is small or even to zero while in the rotated form this angle is at least higher than 90 °. For example the simple $[Fe_2(CO)_6(\mu\text{-pdt})]$ (pdt = $S_2C_3H_6$; propane-1,3-dithiolato) complex exhibits a dihedral angle of 0 ° in the all-terminal CO form and this angle became 96 ° in the corresponding rotated form.[50,51] In **5** and **6** the dihedral angles are determined as 87.1° and 23.8 °, respectively.

A summary of the experimental IR spectra in CH_2Cl_2, solid state and the computed CO stretching mode frequencies for $\mathbf{5}_{\mathbf{unrot}}$, $\mathbf{5}_{\mathbf{semirot}}$ and $\mathbf{5}_{\mathbf{rot}}$ are shown in Table 2. On average, the computed IR spectra for $\mathbf{5}_{\mathbf{semirot}}$ and $\mathbf{5}_{\mathbf{unrot}}$ are both in reasonable agreement with the experimental spectrum from CH_2Cl_2 solution, while the formation of $\mathbf{5}_{\mathbf{rot}}$ can be ruled out.

Table 2. Experimental and BP86/TZVP gas-phase computed CO stretching mode frequencies in cm^{-1} (theoretical intensities in km/mol)

IR exp. (CH_2Cl_2 solution)	IR exp. (solid)	$\mathbf{5}_{unrot}$	$\mathbf{5}_{semirot}$	$\mathbf{5}_{rot}$
	1801			1778 (630)
1903	1910	1885 (498)	1903 (752)	1903 (491)
1937	1943	1944 (518)	1904 (391)	1940 (541)
1989	1974	1953 (632)	1953 (612)	1989 (909)
2008	2002	2008 (925)	2000 (788)	

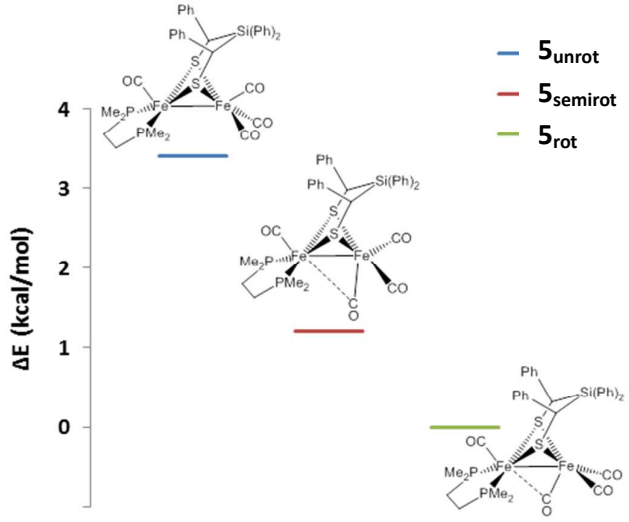

Fig. 6: Total energy differences (in kcal/mol) between $\mathbf{5}_{unrot}$, $\mathbf{5}_{semirot}$ and $\mathbf{5}_{rot}$.

These results highlight a discrepancy between experimental observations and topology of the DFT potential energy surface. To shed some light on such issue, we consider a number of simplified models of molecular systems under investigation. The idea is to probe the effect of each factor (i.e. bridgehead type/size and donor vs acceptor coordination to a single Fe) separately. Therefore, starting from $[Fe_2(CO)_6(\mu\text{-pdt})]$ complex, we first substituted the two terminal equatorial CO with the dmpe ligand and then the propane dithiolato by the silicon based ligand. The $[Fe_2(CO)_6(\mu\text{-pdt})]$ complex has an all terminal energy minimum structure, while the rotated form $\mathbf{pdt}_{rot}$ is a transition state (free energy barrier 11.2 kcal/mol). As aforementioned, the structure of $[Fe_2(CO)_4(\kappa^2\text{-dmpe})(\mu\text{-pdt})]$ (**7**) has been considered (Figure 7),[52] in which the silicon based pendant ligand, present in the original species **5**, is substituted with a propane dithiolato bridge. The rotation of the $Fe(CO)_3$ group is triggered by the dmpe ligand and the lowest energy isomer of **7** has one semi-bridging CO ligand ($\mathbf{7}_{semirot}$), while fully rotated and fully unrotated isomers $\mathbf{7}_{rot}$ and $\mathbf{7}_{unrot}$ are slightly higher in energy. The energy difference among the three isomers suggests that PES of **7** is extremely flat and this makes the case very complicated. Indeed the X ray crystal structure of this species shows a full unrotated (eclipsed) geometry of diiron cluster;[52] our computations suggest that also other isomers might be energy accessible. The coordination around the Fe atom of the lowest energy isomer is similar to that of the $\mathbf{5}_{semirot}$. In this case the C-Fe-Fe-C dihedral angle is 50.2° (Figure 8).

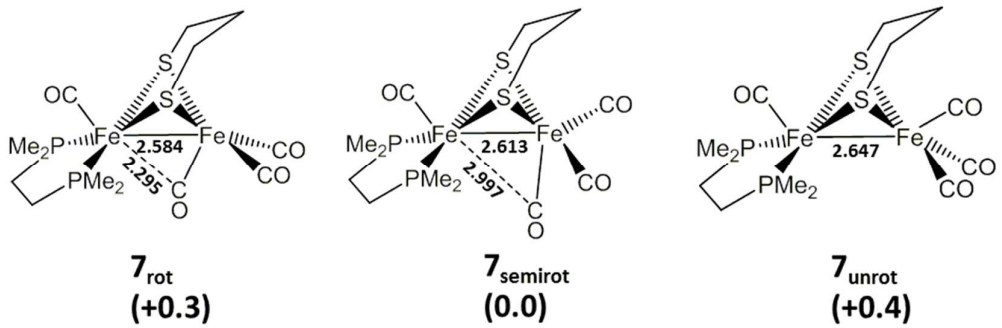

Fig. 7: DFT structures and energies of $[Fe_2(CO)_4](\kappa^2\text{-dmpe})\{\mu\text{-pdt})]$ isomers $\mathbf{7}_{rot}$, $\mathbf{7}_{semirot}$ and $\mathbf{7}_{unrot}$. Distances in Å, energy differences in kcal/mol with respect to $\mathbf{7}_{semirot}$.

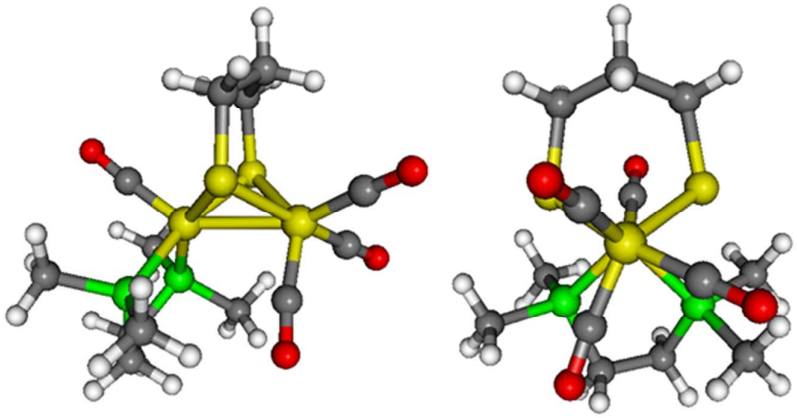

Fig. 8. DFT structure of $\mathbf{7}_{semirot}$. On the right is evidenced the partial rotation of the $Fe(CO)_3$ group with respect to the Fe(dmpe)CO group.

$\mathbf{7}_{semirot}$ was figured out as the most stable isomer at different levels of theory (except for COSMO computation in implicit CH_2Cl_2 solvent). In Table 3 are summarized the various results obtained.

Table 3. Total energy differences (in kcal/mol) between $\mathbf{7}_{rot}$ and $\mathbf{7}_{semirot}$ as a function of the computational level.

	BP86/gas-phase	BP86/CH_2Cl_2	BP86/D3	B3LYP/gas-phase
$\mathbf{7}_{rot}$	+0.3	0.0	+1.4	+1.1
$\mathbf{7}_{semirot}$	0.0	+0.8	0.0	0.0

The second simplified model, considered to investigate the effect of the bulk of the dithiolate bridgehead, is complex **3** and its rotated structure $\mathbf{3}_{rot}$, both sketched in Figure 9. At the BP86 gas-phase level, the all terminal CO isomer $\mathbf{3}_{unrot}$ is the most stable form and the rotated isomer $\mathbf{3}_{rot}$ is a transition state 5.2 kcal/mol higher in energy. Compared with $[Fe_2(CO)_6(\mu\text{-pdt})]$ species, for which the energy difference between rotated and unrotated form is 8.8 kcal/mol, the same difference for complex **3** decreases by 3.6 kcal/mol.

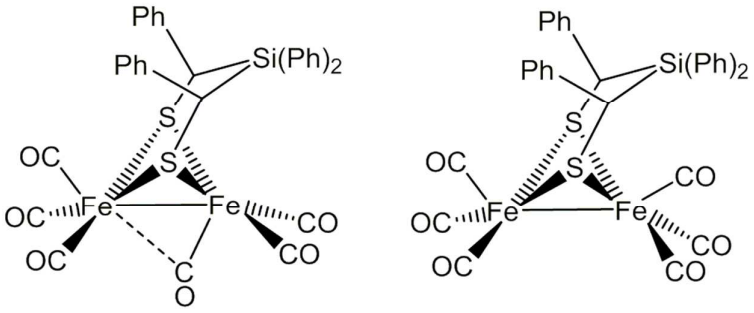

Fig. 9: Complex **3** (right) with its simplified considered rotated structure $\mathbf{3}_{rot}$ (left).

Based purely upon DFT computations for simplified $\mathbf{pdt}_{rot}$ and $\mathbf{7}_{rot}$ models, we conclude that the dmpe ligand provides a large contribution toward stabilization of the rotated/semi-rotated form, while the bridgehead bulk/size plays an apparently minor role (although a measurable one).

In the crystal structure of **5** the distance from the Fe1 atom, which is in a semi-rotated environment, to the closest aromatic CH bond is too long to be considered even a remote agostic or anagostic interaction, i.e. endowed of purely electrostatic character (unlike stronger agostic interactions, having "2-electron-3-centers" character).[53,54] This is in close agreement with recent works suggesting that without a subtle stabilizing effect arising from a remote agostic interaction established intramolecularly, the full-rotated geometry is not favoured and semirotated structures, like in **5**, are observed.[23,24,36] Nevertheless, since DFT optimization of **5** (see Figure 5 and preceding discussion) has shown a shortening of the interatomic Fe···H-C distance down to about 2.9 Å (i.e., the upper limit reported for distances associated with anagostic interactions,[53] we have investigated computationally the effect(s) of the solvent (acetonitrile, implicit model) and of the dispersion (within DFT-D3 empirical dispersion correction for DFT calculations)[55] on the Fe···H-C distance. In Figure 10 are reported the values of the Fe···H distance and of the Fe···H-C angle upon variation of the level of theory. If implicit solvatation is considered, the Fe···H distance decreases by 0.061 Å while the decrease is only 0.024 Å when taking into account the dispersion. These results confirm that dispersion and solvent inclusion in the computational model do not alter significantly the original result obtained in gas phase conditions. They further suggest that, although an evident shortening of the Fe···H-C distance is observed in silicon respect to the molecular structure (possibly due to neglecting packing forced by the computational model) yet such value is still very close to the upper limit indicated in literature for the agostic interactions. This also indicates that the boundaries between semi-rotated and full rotated structures may be governed by a weak but crucial effect. [23,24,36]

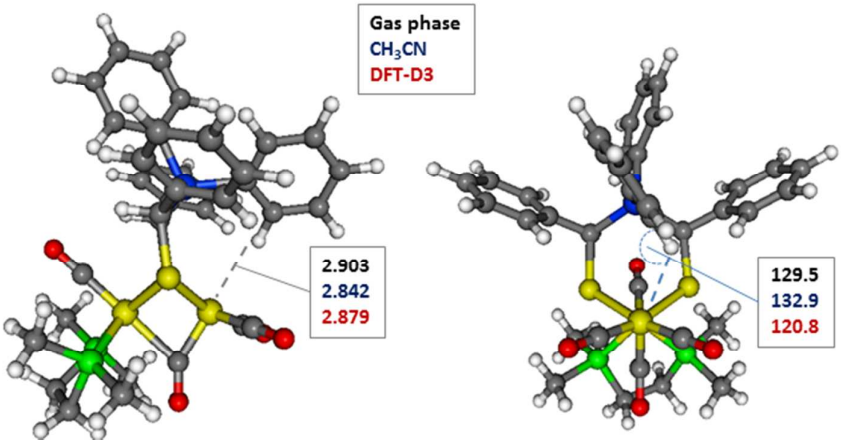

Fig 10: Values observed computationally of the Fe···H distance (Å) and the Fe···H-C angle (°) upon variation of the level of theory for complex **5** (in black gas-phase level, in blue implicit CH_3CN COSMO solvatation, in red DFT using D3 dispersion correction).

Electrochemical studies of 3, 5 and 6

The cyclic voltammetry of **3** shows a quasi-reversible reduction at $E_{1/2}^{red}$ = -1.57 V in CH_2Cl_2 – $[NBu_4][PF_6]$, (Figure 11), at $E_{1/2}^{red1}$ = -1.43 V in MeCN–$[NBu_4][PF_6]$. The comparison of the reduction potential of **3** with that of a Si-containing hexacarbonyl analogue ($E_{1/2}^{red}$ = -1.55 V),[35] measured under identical experimental conditions in CH_2Cl_2-$[NBu_4][PF_6]$, indicates that the electronic effects of the two Si-containing bridges are similar. Moreover, the scan rate dependence of the current function ($i_p^{red}/v^{1/2}$ C) of **3** follows the same trend as for the $[Fe_2(CO)_6\{\mu\text{-}(SCH_2)_2R\}]$ (R = 1-silafluorenyl, $C_{12}H_8Si$) complex (ESI, Figure S1), which suggests that both compounds reduce according to similar mechanisms.[35] Thus, at slow scan rates, the reduction involves the transfer of two electrons according to the ECE process shown in Scheme 3.

$$3 \underset{}{\overset{1e^-}{\rightleftharpoons}} 3^- \underset{k_b}{\overset{k_f}{\rightleftharpoons}} (3')^- \overset{1e^-}{\rightleftharpoons} (3')^{2-}$$

E1 = -1.57 V ; E2 - E1 > 0

Scheme 3 : Proposed ECE mechanism for the reduction of **3**.

Upon raising the scan rate, the intervening chemical step is suppressed and the current measured at fast scan rates corresponds to the transfer of a single electron (ESI, Figure S1) at $E_{1/2}$ = -1.57 V (Figure 11, v = 5 Vs^{-1}). The reduction of related diiron dithiolate complexes, either in a single two-electron EE process,[16,56–61] or according to an ECE mechanism generally results in the cleavage of a Fe-S bond and the shift of a CO group from a terminal to a bridging position.[32,35,62–68] In the present case, the large peak separation (ΔE_p) of the reduction at fast scan rates suggests that it is not entirely reversible electrochemically, so that some structure change might take place concomitantly with the electron transfer step.[63]

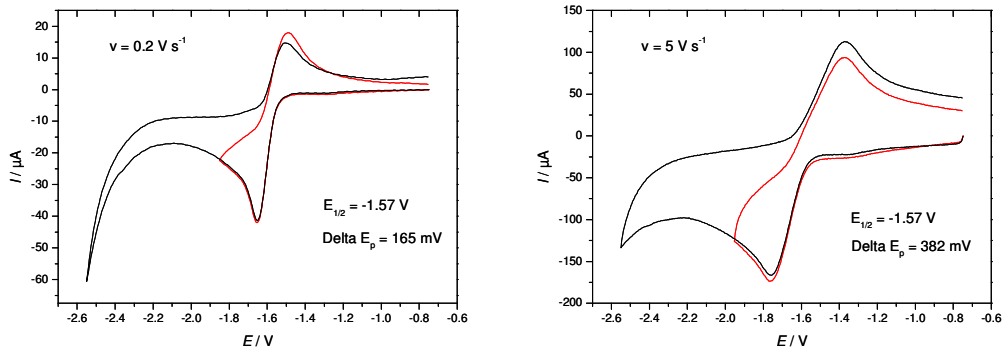

Fig. 11: Cyclic voltammetry of **3**, 0.9 mM in CH_2Cl_2-$[NBu_4][PF_6]$ (potentials are in V vs Fc^+/Fc).

As expected, and in accordance with the IR data, the substitution of two COs by the dmpe ligand into the hexacarbonyl complex **3** shifts the reduction potential to more negative values, respectively 0.63 and 0.74 V for the chelated complex **5** (E_p^{red1} = -2.21 V in CH_2Cl_2-$[NBu_4][PF_6]$) and the bridged complex **6** (E_p^{red1} = -2.32 V in CH_2Cl_2-$[NBu_4][PF_6]$) (ESI, Figure S2).

Recently, it has been demonstrated that the electrochemical reduction of $[Fe_2(CO)_4(\kappa^2\text{-dmpe})\{\mu\text{-}(SCH_2)_2NBn\}]$,[36] as that of other chelated compounds $[Fe_2(CO)_4(\kappa^2\text{-dppe})(\mu\text{-}SCH_2XCH_2S)]$ (X = CH_2, N-^{i}Pr; N-Bn; N-$CH_2CH_2OCH_3$),[41] gives rise to an electron-transfer catalyzed (ETC) isomerisation to the bridged analogue. In the case of **5**, no ETC process could be detected. Indeed, while **6** reduces at E_p^{red1} = -2.14 V in MeCN-$[NBu_4][PF_6]$ (ESI, Figure S3), the irreversible reduction of **5** at E_p^{red1} = -2.00 V is followed by a second reduction at E_p^{red2} = -2.30 V, which indicates that the reduction of **5** does not generate the complex **6**. In contrast to the occurrence of an ETC isomerisation when the dmpe ligand is associated to the propanedithiolate bridge,[41] no such process is observed for **5,** which possesses a dithiolate Si-bridge. The way the S-to-S link may hinder the migration of one end of the diphosphine ligand from a metal center to the other is not presently understood.

Conclusion

In summary, we report on the reaction of complex **3** with one and two equivalents of dmpe, respectively, leading to the three different compounds **4**, **5** and **6**. The complexes were characterized by X-ray diffraction. The molecular structure of the $[Fe^IFe^I]$ hydrogenase model complex **5** shows that the introduction of the bidendate phosphine dmpe enforces a semi-rotated conformation in solid state. The identification of this species with its structural features, along with DFT computations, supports the idea that in order to obtain a fully rotated geometry related to the active site of $[Fe^IFe^I]$ hydrogenase three factors are important: (a) asymmetrical coordination at the two iron atoms using a bidentate donor ligand, here dmpe, (b) a bulky dithiolato bridgehead, which promotes (c) a weak remote agostic Fe···H-C interaction. Indeed each of these three factors seems to be crucial for observing, in dithiolate models, a full-rotated geometry, as that existing in the [FeFe] hydrogenase cofactor. To date, when one of these factors is not conformed, only partially or semi-rotated structures of [FeFe] hydrogenase models like complex **5** have been observed.[14] On the other hand, a glance to the rotated state of the natural cofactor reveals that no type of agostic interaction is necessary to obtain the full-rotated geometry. The amino acid residues, which face the [2Fe2S] cluster and the [4Fe4S] cubane, are able to constrain the H-cluster itself in the full-rotated form.[69] Thus in nature, just (a) and (b) of the established factors are necessary, which suggests the importance of a sterical demanding environment around the diiron center of [FeFe] hydrogenase model complexes by dithiolato ligands to force a full-rotated geometry. With the herein reported complex **5**, we could show an example with the highest degree of rotation so far reported for $[Fe^IFe^I]$ hydrogenase models without any agostic interactions (Fe···H-C)[14] and enabling new approaches for the design of dithiolato bridgeheads to achieve a full-rotated geometry related to the active site of [Fe–Fe] hydrogenases without any type of H-bond interaction.

Acknowledgment

Financial support for this work was provided by the Deutsche Bundesstiftung Umwelt (to R. Goy) and the Studienstiftung des Deutschen Volkes, the Alexander-von-Humboldt foundation as well as the Fonds of the Chemical Industry (to U.-P. Apfel). We are grateful to Dr. F. Michaud for crystallographic measurements. The Centre National de la Recherche Scientifique (CNRS), the University of Brest and the University of Milano Bicocca are acknowledged for financial support.

Notes and references

[a] Institut für Anorganische und Analytische Chemie, Friedrich-Schiller-Universität, Humboldtstraße 8, 07743 Jena, E-mail: wolfgang.weigand@uni-jena.de
[b] Inorganic Chemistry I / Bioinorganic Chemistry, Ruhr-Universität Bochum, Universitätsstraße 150, 44780 Bochum, Germany, E-mail: ulf.apfel@rub.de

[c] Department of Biotechnology and Biosciences, University of Milano-Bicocca, 20126 Milan, Italy, E-mail: luca.degioia@unimib.it
[d] University of Brest; CNRS, UMR 6521 « Chimie, Electrochimie Moléculaires et Chimie Analytique », CS 93837, 29238 Brest-Cedex 3, France. Email: Philippe.Schollhammer@univ-brest.fr
[e] Jena Center for Soft Matter (JCSM), Philosophenweg 7, 07743 Jena, Germany

Electronic Supplementary Information (ESI) available: See DOI: 10.1039/b000000x/

1. C. Madden, M. D. Vaughn, I. Díez-Pérez, K. A. Brown, P. W. King, D. Gust, A. L. Moore and T. A. Moore, *J. Am. Chem. Soc.*, 2012, **134**, 1577–1582.
2. D. J. Evans and C. J. Pickett, *Chem. Soc. Rev.*, 2003, **32**, 268–275.
3. A. Volbeda and J. Fontecillacamps, *Coord. Chem. Rev.*, 2005, **249**, 1609–1619.
4. T. Liu and M. Y. Darensbourg, *J. Am. Chem. Soc.*, 2007, **129**, 7008–7009.
5. M. L. Singleton, N. Bhuvanesh, J. H. Reibenspies and M. Y. Darensbourg, *Angew. Chem.*, 2008, **120**, 9634–9637.
6. M. L. Singleton, R. M. Jenkins, C. L. Klemashevich and M. Y. Darensbourg, *Comptes Rendus Chim.*, 2008, **11**, 861–874.
7. M. L. Singleton, N. Bhuvanesh, J. H. Reibenspies and M. Y. Darensbourg, *Angew. Chem. Int. Ed.*, 2008, **47**, 9492–9495.
8. J.-F. Capon, F. Gloaguen, F. Y. Pétillon, P. Schollhammer and J. Talarmin, *Coord. Chem. Rev.*, 2009, **253**, 1476–1494.
9. M. K. Harb, J. Windhager, A. Daraosheh, H. Görls, L. T. Lockett, N. Okumura, D. H. Evans, R. S. Glass, D. L. Lichtenberger, M. El-khateeb and W. Weigand, *Eur. J. Inorg. Chem.*, 2009, 3414–3420.
10. M. K. Harb, U.-P. Apfel, J. Kübel, H. Görls, G. A. N. Felton, T. Sakamoto, D. H. Evans, R. S. Glass, D. L. Lichtenberger, M. El-khateeb and W. Weigand, *Organometallics*, 2009, **28**, 6666–6675.
11. C. Tard and C. J. Pickett, *Chem. Rev.*, 2009, **109**, 2245–2274.
12. M. Y. Darensbourg and W. Weigand, *Eur. J. Inorg. Chem.*, 2011, 994–1004.
13. S. Tschierlei, S. Ott and R. Lomoth, *Energy Environ. Sci.*, 2011, **4**, 2340–2352.
14. C.-H. Hsieh, Ö. F. Erdem, S. D. Harman, M. L. Singleton, E. Reijerse, W. Lubitz, C. V. Popescu, J. H. Reibenspies, S. M. Brothers, M. B. Hall and M. Y. Darensbourg, *J. Am. Chem. Soc.*, 2012, **134**, 13089–13102.
15. N. Wang, M. Wang, L. Chen and L. Sun, *Dalton Trans.*, 2013, **42**, 12059–12071.
16. R. Trautwein, L. R. Almazahreh, H. Görls and W. Weigand, *Z. Für Anorg. Allg. Chem.*, 2013, **639**, 1512–1519.
17. T. R. Simmons, G. Berggren, M. Bacchi, M. Fontecave and V. Artero, *Coord. Chem. Rev.*, 2014, **270-271**, 127–150.
18. D. Zheng, M. Wang, L. Chen, N. Wang and L. Sun, *Inorg. Chem.*, 2014, **53**, 1555–1561.
19. B. J. Lemon and J. W. Peters, *Biochemistry (Mosc.)*, 1999, **38**, 12969–12973.
20. A. S. Pandey, T. V. Harris, L. J. Giles, J. W. Peters and R. K. Szilagyi, *J. Am. Chem. Soc.*, 2008, **130**, 4533–4540.
21. Y. Nicolet, A. L. de Lacey, X. Vernède, V. M. Fernandez, E. C. Hatchikian and J. C. Fontecilla-Camps, *J. Am. Chem. Soc.*, 2001, **123**, 1596–1601.
22. A. L. De Lacey, V. M. Fernández, M. Rousset and R. Cammack, *Chem. Rev.*, 2007, **107**, 4304–4330.
23. S. Munery, J.-F. Capon, L. De Gioia, C. Elleouet, C. Greco, F. Y. Pétillon, P. Schollhammer, J. Talarmin and G. Zampella, *Chem. - Eur. J.*, 2013, **19**, 15458–15461.
24. W. Wang, T. B. Rauchfuss, C. E. Moore, A. L. Rheingold, L. De Gioia and G. Zampella, *Chem. - Eur. J.*, 2013, **19**, 15476–15479.
25. D. J. Crouthers, J. A. Denny, R. D. Bethel, D. G. Munoz and M. Y. Darensbourg, *Organometallics*, 2014, **33**, 4747–4755.
26. D. Zheng, M. Wang, L. Chen, N. Wang, M. Cheng and L. Sun, *Chem. Commun.*, 2014, **50**, 9255–9258.
27. A. Silakov, E. J. Reijerse, S. P. J. Albracht, E. C. Hatchikian and W. Lubitz, *J. Am. Chem. Soc.*, 2007, **129**, 11447–11458.
28. A. Adamska, A. Silakov, C. Lambertz, O. Rüdiger, T. Happe, E. Reijerse and W. Lubitz, *Angew. Chem. Int. Ed.*, 2012, **51**, 11458–11462.
29. A. Adamska-Venkatesh, D. Krawietz, J. Siebel, K. Weber, T. Happe, E. Reijerse and W. Lubitz, *J. Am. Chem. Soc.*, 2014, 140729162153007.
30. J. Esselborn, C. Lambertz, A. Adamska-Venkatesh, T. Simmons, G. Berggren, J. Noth, J. Siebel, A. Hemschemeier, V. Artero, E. Reijerse, M. Fontecave, W. Lubitz and T. Happe, *Nat. Chem. Biol.*, 2013, **9**, 607–609.
31. G. Berggren, A. Adamska, C. Lambertz, T. R. Simmons, J. Esselborn, M. Atta, S. Gambarelli, J.-M. Mouesca, E. Reijerse, W. Lubitz, T. Happe, V. Artero and M. Fontecave, *Nature*, 2013, **499**, 66–69.
32. U.-P. Apfel, D. Troegel, Y. Halpin, S. Tschierlei, U. Uhlemann, H. Görls, M. Schmitt, J. Popp, P. Dunne, M. Venkatesan, M. Coey, M. Rudolph, J. G. Vos, R. Tacke and W. Weigand, *Inorg. Chem.*, 2010, **49**, 10117–10132.
33. U.-P. Apfel, H. Görls, G. A. N. Felton, D. H. Evans, R. S. Glass, D. L. Lichtenberger and W. Weigand, *Helv. Chim. Acta*, 2012, **95**, 2168–2175.
34. U.-P. Apfel, Y. Halpin, H. Görls, J. G. Vos and W. Weigand, *Eur. J. Inorg. Chem.*, 2011, **2011**, 581–588.
35. R. Goy, U.-P. Apfel, C. Elleouet, D. Escudero, M. Elstner, H. Görls, J. Talarmin, P. Schollhammer, L. González and W. Weigand, *Eur. J. Inorg. Chem.*, 2013, 4466–4472.
36. L. De Gioia, C. Elleouet, S. Munery, F. Y. Pétillon, P. Schollhammer, J. Talarmin and G. Zampella, *Eur. J. Inorg. Chem.*, 2014, **22**, 3456–3461.
37. J. Zubieta, E. Block, G. Ofori-Okai and K. Tang, *Inorg. Chem.*, 1990, **29**, 4595–4597.
38. R. S. Glass, N. E. Gruhn, E. Lorance, M. S. Singh, N. Y. T. Stessman and U. I. Zakai, *Inorg. Chem.*, 2005, **44**, 5728–5737.
39. W. Gao, J. Ekström, J. Liu, C. Chen, L. Eriksson, L. Weng, B. Åkermark and L. Sun, *Inorg. Chem.*, 2007, **46**, 1981–1991.
40. J.-F. Capon, F. Gloaguen, F. Y. Pétillon, P. Schollhammer and J. Talarmin, *Eur. J. Inorg. Chem.*, 2008, 4671–4681.
41. S. Ezzaher, J.-F. Capon, F. Gloaguen, F. Y. Pétillon, P. Schollhammer and J. Talarmin, *Inorg. Chem.*, 2007, **46**, 9863–9872.
42. F. I. Adam, G. Hogarth and I. Richards, *J. Organomet. Chem.*, 2007, **692**, 3957–3968.
43. A. Tsuboyama, K. Kuge, M. Furugori, S. Okada, M. Hoshino and K. Ueno, *Inorg. Chem.*, 2007, **46**, 1992–2001.
44. F. I. Adam, G. Hogarth, S. E. Kabir and I. Richards, *Comptes Rendus Chim.*, 2008, **11**, 890–905.

45. N. Wang, M. Wang, T. Liu, P. Li, T. Zhang, M. Y. Darensbourg and L. Sun, *Inorg. Chem.*, 2008, **47**, 6948–6955.
46. S. Ghosh, G. Hogarth, N. Hollingsworth, K. B. Holt, I. Richards, M. G. Richmond, B. E. Sanchez and D. Unwin, *Dalton Trans.*, 2013, **42**, 6775.
47. S. Ghosh, G. Hogarth, N. Hollingsworth, K. B. Holt, S. E. Kabir and B. E. Sanchez, *Chem. Commun.*, 2014, **50**, 945.
48. A. W. Addison, T. N. Rao, J. Reedijk, J. van Rijn and G. C. Verschoor, *J. Chem. Soc. Dalton Trans.*, 1984, 1349–1356.
49. M. Brookhart, M. L. H. Green and G. Parkin, *Proc. Natl. Acad. Sci.*, 2007, **104**, 6908–6914.
50. E. J. Lyon, I. P. Georgakaki, J. H. Reibenspies and M. Y. Darensbourg, *J. Am. Chem. Soc.*, 2001, **123**, 3268–3278.
51. L. Bertini, C. Greco, P. Fantucci and L. De Gioia, *Int. J. Quantum Chem.*, 2014, 1–11.
52. S. Ezzaher, J.-F. Capon, F. Gloaguen, N. Kervarec, F. Y. Pétillon, R. Pichon, P. Schollhammer and J. Talarmin, *Comptes Rendus Chim.*, 2008, **11**, 906–914.
53. D. Braga, F. Grepioni, E. Tedesco, K. Biradha and G. R. Desiraju, *Organometallics*, 1997, **16**, 1846–1856.
54. M. G. Derry Holaday, G. Tarafdar, A. Kumar, M. L. P. Reddy and A. Srinivasan, *Dalton Trans.*, 2014, **43**, 7699–7703.
55. S. Grimme, *J. Comput. Chem.*, 2004, **25**, 1463–1473.
56. D. T. Pierce and W. E. Geiger, *J. Am. Chem. Soc.*, 1992, **114**, 6063–6073.
57. F. A. Schultz, *J. Solid State Electrochem.*, 2011, **15**, 1833–1843.
58. R. L. Lord, F. A. Schultz and M.-H. Baik, *Inorg. Chem.*, 2010, **49**, 4611–4619.
59. D. Uhrhammer and F. A. Schultz, *J. Phys. Chem. A*, 2002, **106**, 11630–11636.
60. J. B. Fernandes, L. Q. Zhang and F. A. Schultz, *J. Electroanal. Chem. Interfacial Electrochem.*, 1991, **297**, 145–161.
61. D. H. Evans, *Chem. Rev.*, 2008, **108**, 2113–2144.
62. J.-F. Capon, F. Gloaguen, P. Schollhammer and J. Talarmin, *J. Electroanal. Chem.*, 2004, **566**, 241–247.
63. G. A. N. Felton, A. K. Vannucci, J. Chen, L. T. Lockett, N. Okumura, B. J. Petro, U. I. Zakai, D. H. Evans, R. S. Glass and D. L. Lichtenberger, *J. Am. Chem. Soc.*, 2007, **129**, 12521–12530.
64. J. Windhager, M. Rudolph, S. Bräutigam, H. Görls and W. Weigand, *Eur. J. Inorg. Chem.*, 2007, 2748–2760.
65. J.-F. Capon, S. Ezzaher, F. Gloaguen, F. Y. Pétillon, P. Schollhammer, J. Talarmin, T. J. Davin, J. E. McGrady and K. W. Muir, *New J. Chem.*, 2007, **31**, 2052–2064.
66. G. A. N. Felton, B. J. Petro, R. S. Glass, D. L. Lichtenberger and D. H. Evans, *J. Am. Chem. Soc.*, 2009, **131**, 11290–11291.
67. E. S. Donovan, G. S. Nichol and G. A. N. Felton, *J. Organomet. Chem.*, 2013, **726**, 9–13.
68. It must be noted that the uncompensated solution resistance certainly contributes to the large ΔEp at fast scan rates.
69. A. R. Finkelmann, M. T. Stiebritz and M. Reiher, *Chem. Sci.*, 2014, **5**, 215–221.

TOC

Semi-rotated state – As the first example so far a [$Fe^{I}Fe^{I}$] H_2ase model complex with a bulky silicon-containing dithiolate bridge is reported showing a semi-rotated geometry without the need of stabilization via agostic interactions.

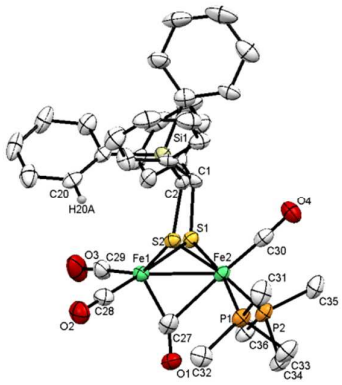

Roman Goy, Luca Bertini*, Catherine Elleouet, Helmar Görls, Giuseppe Zampella, Jean Talarmin, Luca De Gioia*, Philippe Schollhammer*, Ulf-Peter Apfel*, Wolfgang Weigand*

Page No. – Page No.

A Sterically Stabilized Fe^{I}-Fe^{I} Semi-Rotated Conformation of [FeFe] Hydrogenase Subsite Model